Advanced Composites and Hybrid Materials (2021) 4:1166–1175
https://doi.org/10.1007/s42114-021-00349-3

ORIGINAL RESEARCH

Synchronously improved wave-transparent performance and mechanical properties of cyanate ester resins via introducing fluorine-containing linear random copolymer

Yuxiao Zhou[1] · Junliang Zhang[1] · Chang Qu[2] · Liangchen Li[2] · Jie Kong[1] · Junwei Gu[1]

Received: 31 August 2021 / Revised: 14 September 2021 / Accepted: 16 September 2021 / Published online: 2 October 2021

Abstract

A novel epoxy and fluorine-containing linear random copolymer of P(PFS-*co*-GMA) is synthesized from pentafluorostyrene (PFS) and glycidyl methacrylate (GMA) via RAFT polymerization, which is then performed to prepare modified bisphenol A dicyanate ester (*m*-BADCy) resin. Small dipole and low polarizability of C–F bond in PFS improve the wave-transparent performance of *m*-BADCy resin. Besides, the large free volume of P(PFS-*co*-GMA) and formation of semi-IPN structure simultaneously enhances the mechanical properties. The obtained *m*-BADCy resin with 15 wt% P(PFS-*co*-GMA) demonstrated the optimal comprehensive properties. ε and tanδ were 2.59 and 0.0053, respectively, lower than that of pure BADCy resin (2.97 and 0.0090). The corresponding wave transmittance ($|T|^2$) increased from 92.9% of pure BADCy resin to 94.5%. Meanwhile, the corresponding flexural and impact strength increased to 122.4 MPa and 14.6 kJ/m^2, increased by 23.1% and 49.0% compared with pure BADCy resin (99.4 MPa and 9.8 kJ/m^2), respectively.

Keywords Bisphenol A dicyanate ester · Epoxy and fluorine-containing linear random copolymer · Dielectric properties · Mechanical properties

1 Introduction

Compared with those of epoxy resins [1], polyimide [2], and bismaleimide [3], cyanate ester (CE) resins possess lots of unique properties as a high-performance resin matrix in polymer composites [4–6]. CE resins can keep low and stable dielectric constant (ε, 2.8 ~ 3.2) and dielectric loss tangent (tanδ, 0.002 ~ 0.008) across a wide range of temperature (0 ~ 220 °C) and frequency (0 ~ 10^{11} Hz) [7–9]. Besides, CE resins also display high thermal stability, low moisture absorption, good processability, etc. Therefore, CE resins have been widely used in microelectronics industry and aerospace, especially high-speed printed circuit boards, satellite antenna system, and radomes [10–12]. However, the dielectric properties of CE resins need to be improved in order to achieve higher wave-transparent performance for the electromagnetic waves. Besides, the toughness of CE resins after curing is relatively poor due to the symmetrical triazine structures [13, 14]. Therefore, to meet the growing demand for high-performance wave-transparent materials, it is urgent to prepare CE resins with excellent wave-transparent performance and mechanical properties while maintaining excellent thermal stability.

Presently, two strategies have been discovered to prepare CE resin showing excellent wave-transparent performance (equal to low ε and tanδ) [15–17]. One is to introduce inorganic particles with hollow structure (such as silsesquioxane (SSQ) [18, 19] and porous silica (SiO_2) [20, 21]) to reduce the number of polarized molecules per unit volume, thereby reducing the ε and tanδ of CE resin. Zhang et al. [19] introduced methyl SSQ (Me-SSQ) to prepare modified CE resin (Me-SSQ/CE). The ε value of Me-SSQ/CE resin containing 20 wt% Me-SSQ decreased to 2.78, lower than that of pure CE resin (3.05). Wu et al. [21] applied mesoporous silica

✉ Junliang Zhang
junliang.zhang@nwpu.edu.cn

✉ Junwei Gu
gjw@nwpu.edu.cn; nwpugjw@163.com

[1] Shaanxi Key Laboratory of Macromolecular Science and Technology, School of Chemistry and Chemical Engineering, Northwestern Polytechnical University, Xi'an, Shaanxi 710072, People's Republic of China

[2] Queen Mary University of London Engineering School, Northwestern Polytechnical University, Xi'an, Shaanxi 710072, People's Republic of China

(MPS) and glycidyl polyhedral oligomeric silsesquioxane (G-POSS) to modify CE resin. The obtained modified CE resin with 4 wt% POSS-MPS displayed low ε and tanδ of 2.78 and 0.0079, 15% and 34% lower than those of pure CE resin. Although the ε and tanδ values can be reduced by introducing hollow structures, the process is relatively complicated as pre-treatment is always required to improve the compatibility of inorganic particles with CE resin to avoid agglomeration. Moreover, introduction of hollow structure into CE resin will adversely affect their mechanical and thermal properties [22–24].

The other way is to add small molecules or polymers with low-polar groups such as O–Si [25, 26], C–Si [27, 28], and C–F [29–31] into CE resin. Liu et al. [25] obtained modified epoxy resin/cyanate ester (eCE) by adding liquid crystal hyperbranched polysiloxane (LCPSi). The ε and tanδ values of the LCPSi/eCE resin with 1.5 wt% LCPSi decreased to approximately 78% and 45% of pure eCE resin, respectively. Mathivathanan et al. [28] prepared PDMS-OCN/DGEBA polymer matrix by copolymerizing polydimethylsiloxane terminated cyanate ester (PDMS-OCN) with diglycidyl ether of bisphenol A (DGEBA). The obtained PDMS-OCN/DGEBA showed low ε (2.75) due to the existence of the less polar group of C–Si bond. In our previous work [32], a fluorine-containing and epoxy-terminated polyaryletherketone (EFPAEK) was introduced into the bisphenol A dicyanate ester (BADCy) resin to prepare EFPAEK/BADCy resin. EFPAEK/BADCy resin with 20 wt% EFPAEK showed the lowest ε of 2.64 under 1 MHz, much lower than that of pure BADCy resin (3.09). Besides, introducing small molecules or polymers with O–Si, C–Si, and C–F groups into the CE resins could simultaneously improve the mechanical and thermal properties of CE resins [33, 34].

Polymers containing pentafluorostyrene (PFS) present superior hydrophobicity [35], excellent thermal stability [36, 37], and chemical resistance. Besides, PFS-containing polymers exhibit ultra-low ε and tanδ because of low polarized C–F bond [38, 39]. Bucholz et al. [38] synthesized poly(D,L-lactide-*b*-pentafluorostyrene) diblock copolymer through sequential ring opening and atom transfer radical polymerization. Diblock copolymer with 21.5 vol% poly(D,L-lactide) demonstrated very low ε value of 2.39. Fu et al. [39] prepared a rigid fluorinated polyimide (FPI) with poly(pentafluorostyrene) on the side chain (FPI-*cb*-PFS). The ε value of FPI-*cb*-PFS film could be reduced to 2.1 compared with that of FPI-Br film (3.0). Therefore, introducing polymers with PFS to prepare CE resin with ultra-low ε is feasible.

To our knowledge, the formation of interpenetrating polymer network (IPN) can significantly enhance the mechanical properties of CE resin [40–42]. Liu and coworkers [41] obtained modified BADCy resin having semi-IPN structure through introducing thermoplastic polyimide into BADCy resin. The impact strength was improved by 47 ~ 320% compared with that of pure BADCy resin. In our previous work [43], a linear PBO precursor (*pre*FLPBO) containing fluorine was employed to modify BADCy resin. Due to the formation of semi-IPN structure between *pre*FLPBO and BADCy in the cured BADCy resin network, the mechanical properties were significantly improved. The impact and flexural strength of the modified BADCy resin by 7 wt% *pre*FLPBO increased to 13.87 kJ/m^2 and 126.5 MPa, respectively, enhanced by 40.4% and 23.5% compared to those of pure BADCy resin (9.88 kJ/m^2 and 102.4 MPa).

The low polarized C–F bond would reduce the ε and tanδ values of BADCy resin. Functional groups of epoxy in glycidyl methacrylate (GMA) could react with –OCN groups of BADCy resin and form flexible five-membered ring oxazolidinone to further increase the compatibility with BADCy resin matrix. Semi-IPN structure would enhance the mechanical properties of BADCy resin. The above combined effects would synchronously improve the wave-transparent performance and mechanical properties of BADCy resin. Therefore, in our present work, a novel PFS-containing linear random copolymer of P(PFS-*co*-GMA) was firstly synthesized through reversible addition-fragmentation chain transfer (RAFT) polymerization with PFS and GMA as monomers. P(PFS-*co*-GMA) was then introduced into BADCy resin to prepare modified BADCy (*m*-BADCy) resin. The structure of P(PFS-*co*-GMA) was characterized by proton nuclear magnetic resonance (^{1}H NMR) spectroscopy, ^{13}C NMR spectroscopy, size exclusion chromatography (SEC), and Fourier infrared (FTIR) spectroscopy. The amount of P(PFS-*co*-GMA) affecting on the wave-transparent performance, mechanical properties, and thermal properties of the *m*-BADCy resin was investigated.

2 Experimental section

Main materials and characterization methods are provided in the Supplementary Materials.

2.1 Synthesis of P(PFS-*co*-GMA)

P(PFS-*co*-GMA) was synthesized by RAFT polymerization. Specifically, CTA (0.808 g, 2 mmol), ACCN (97.6 mg, 0.4 mmol), PFS (8.501 g, 43.82 mmol), GMA (0.691 g, 4.87 mmol), 1,3,5-trioxane (internal standard, 0.162 g), and 1,4-dioxane (9.55 mL) were added into a round bottom flask with a magnetic stir bar inside and sealed using a plastic septum. The above mixture was degassed by bubbling nitrogen for about 15 min. Then the flask was put in an oil bath of 80 °C and reacted for 24 h under stirring. The reaction mixture was then cooled in cold water of 0 °C and opened under air. The reaction

mixture was diluted with an appropriate amount of DCM and added dropwise to MeOH to precipitate the polymer. The obtained polymer was dried at 40 °C for 12 h under reduced pressure to afford as a light-yellow powder. The experimental and characterization data of P(PFS-*co*-GMA) are shown in Table S1.

2.2 Preparation of P(PFS-*co*-GMA) modified BADCy (*m*-BADCy) resin

A certain amount of P(PFS-*co*-GMA) was dissolved in an appropriate amount of THF and heated to form a clear solution, which was then mixed and stirred evenly with preheated BADCy resin at 150 °C for 1 h. Then, the above mixture was poured into a preheated mold at 150 °C and degassed under vacuum, followed by the curing procedure of 180 °C/2 h + 200 °C/6 h + 220 °C/2 h. The preparation process of *m*-BADCy resin is shown in Fig. 1.

3 Results and discussions

3.1 Structural characterization of P(PFS-*co*-GMA)

^{1}H NMR and ^{13}C NMR spectra of P(PFS-*co*-GMA) are shown in Fig. 2a and b, respectively. Peaks at 4.17 ~ 2.79 ppm in Fig. 2a are attributed to the five characteristic resonances of the protons for epoxy group. Signals at chemical shift between 2.50 and 0.73 ppm correspond to the protons from the polymer backbone. Peak at 174.60 ppm in Fig. 2b is corresponding to the carbonyl group of GMA while the signals at 146.14 ~ 114.40 ppm are owing to the carbon atoms from benzene ring. Besides, peaks at 65.85, 48.59, and 45.53 ppm belonging to the three carbon atoms of the epoxy group can be observed. Additionally, the signals ascribed to carbon atoms of the polymer backbone are evident between 44.13 and 14.05 ppm. Figure 2c displays the FTIR spectrum of P(PFS-*co*-GMA). Peaks at 2936 and 2858 cm^{-1} are

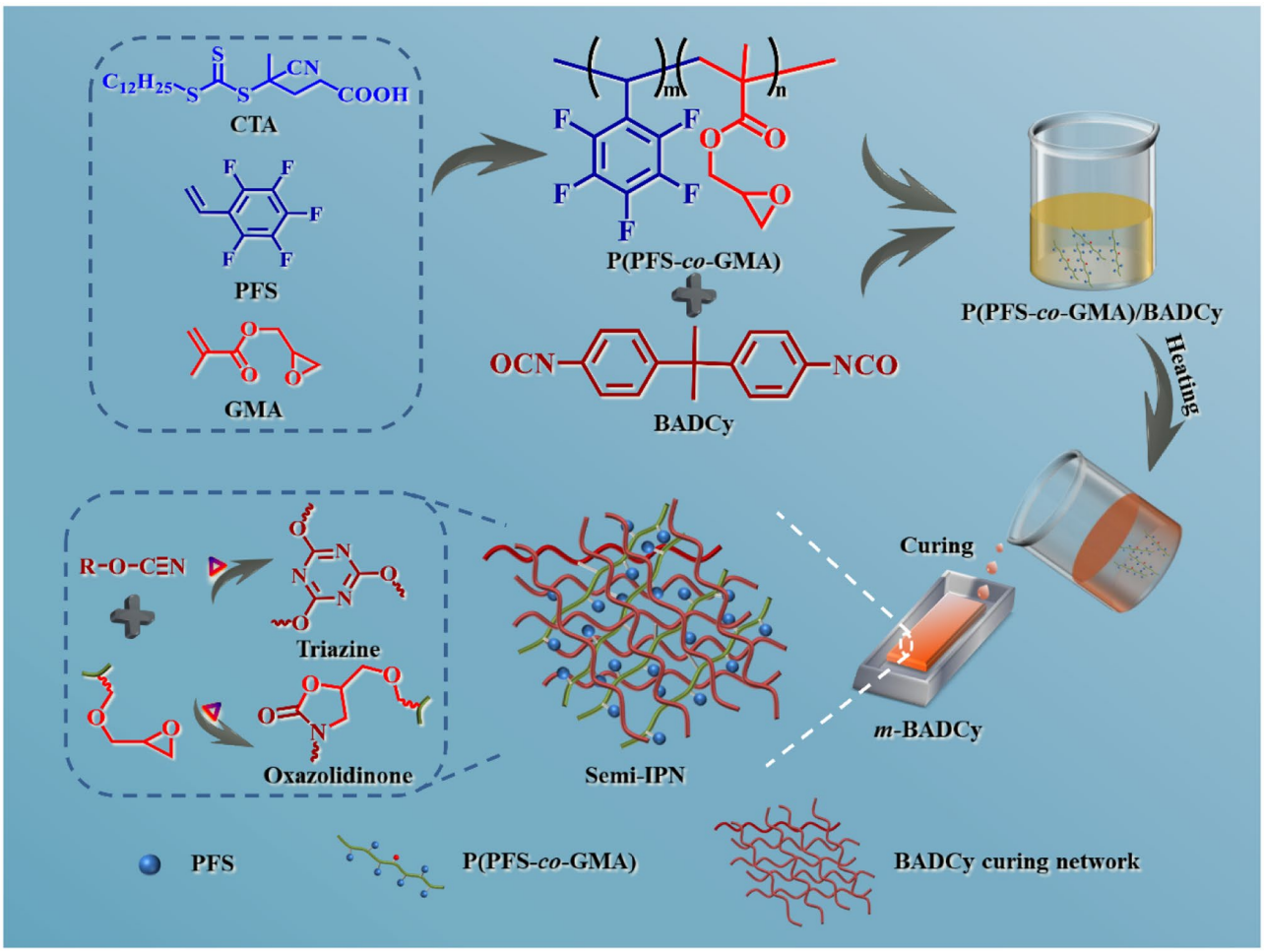

Fig. 1 Schematic diagram of preparation for *m*-BADCy resin

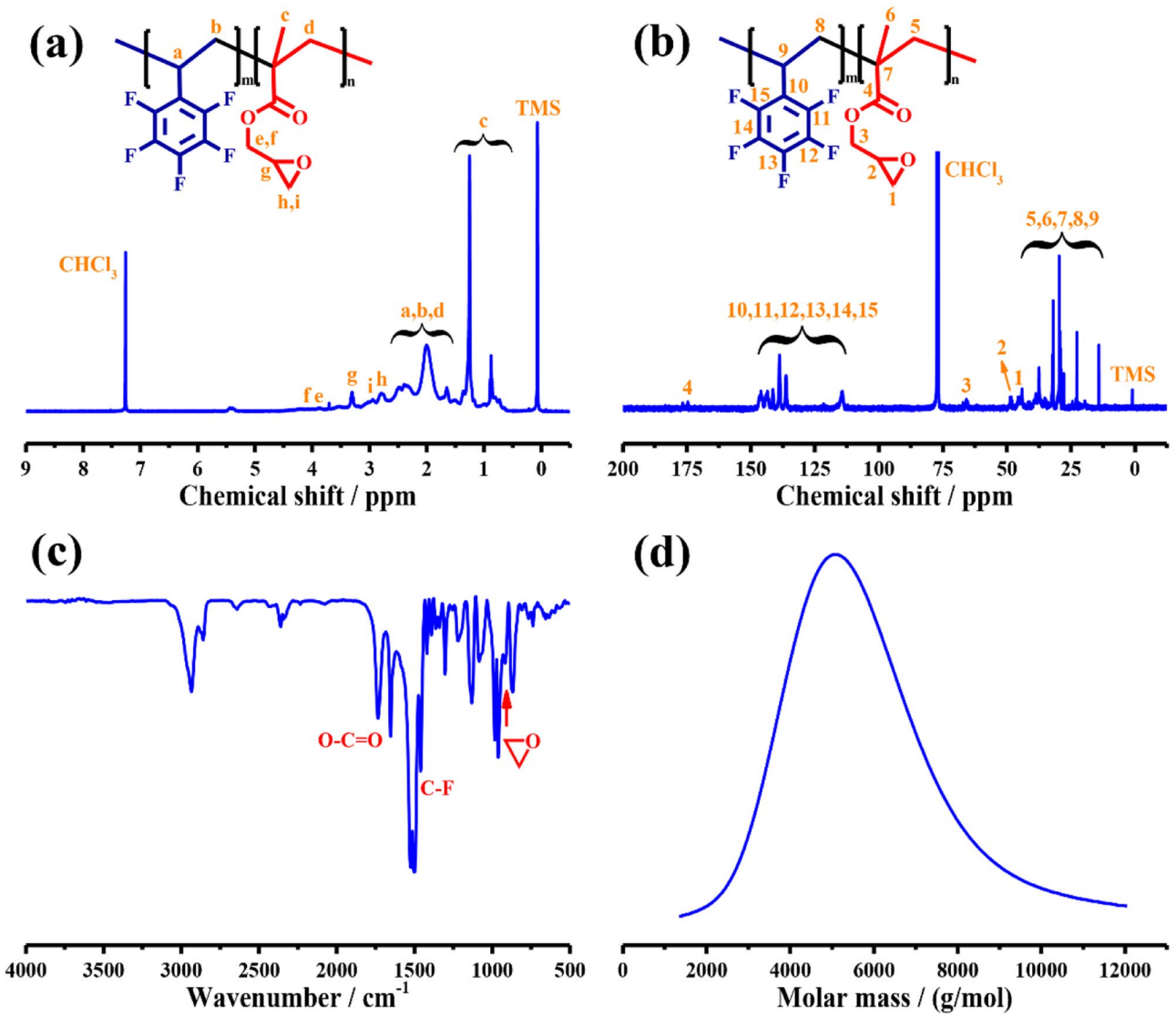

Fig. 2 ^{1}H NMR (**a**), ^{13}C NMR (**b**), FTIR (**c**), and GPC (**d**) spectra of P(PFS-*co*-GMA)

resulted from the characteristic absorption of C–H bond in polymer backbone. The skeleton vibration of the benzene ring and stretching vibration of C–F bond appear at 1653 ~ 1500 cm^{-1} and 1460 ~ 1010 cm^{-1}, respectively. Meanwhile, the absorption at 1734 and 916 cm^{-1} are ascribed to –COO– and epoxy, respectively. NMR and FTIR analyses suggest P(PFS-*co*-GMA) have been synthesized with the expected molecular structure. Figure 2d presents the SEC curve of P(PFS-*co*-GMA), which shows a symmetrical monomodal peak and narrow molar mass distribution ($Đ = 1.11$). The measured number average molar mass ($M_{n,\,SEC}$) is 4700 g/mol, close to the theoretical molar mass ($M_{n,\,th} = 4800$ g/mol), indicating the polymerization is well controlled. The experimental condition for the synthesis and characterization data of P(PFS-*co*-GMA) are also shown in Table S1.

3.2 Wave-transparent performance of *m*-BADCy resin

Figure 3 a and b respectively show the amount of P(PFS-*co*-GMA) affecting on ε and tanδ values of *m*-BADCy resin. Under the same frequency, ε of *m*-BADCy resin firstly decreases and then increases as increasing the amount of P(PFS-*co*-GMA), while the tanδ values remain between 0.0030 and 0.0092. When the content of P(PFS-*co*-GMA) reaches 15 wt%, ε and tanδ values of *m*-BADCy resin at 1 MHz are reduced to the minimum values of 2.59 and 0.0053, respectively, 12.8% and 41.1% lower than that of pure BADCy resin (2.97 and 0.0090). It can be ascribed to the smaller dipole and lower polarizability of the C–F bond in P(PFS-*co*-GMA). Additionally, epoxy groups in GMA will promote the curing reaction of BADCy to aid

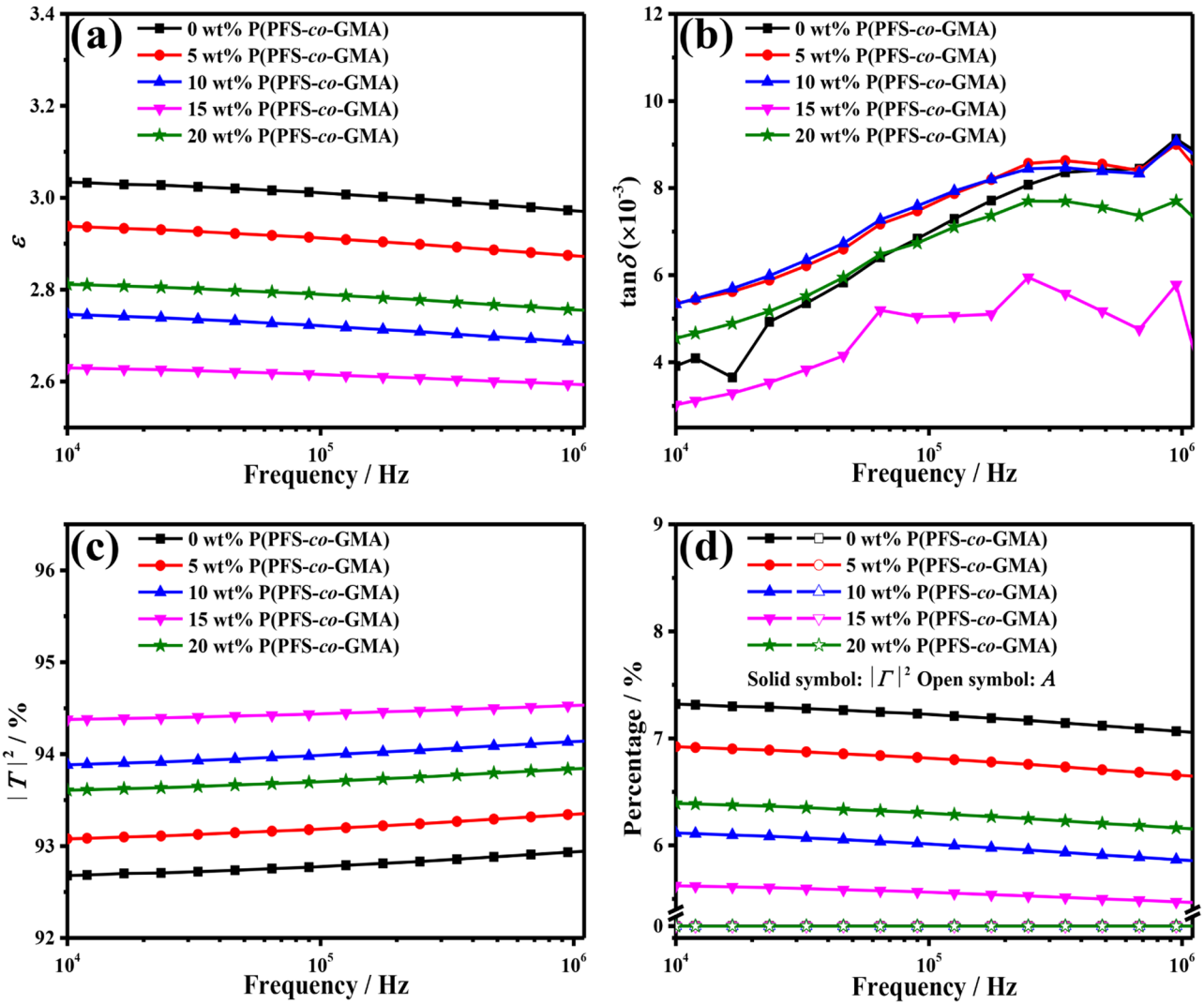

Fig. 3 Effect of P(PFS-*co*-GMA) contents on the ε (**a**), tanδ (**b**), $|T|^2$ (**c**), and $|\Gamma|^2$ and A (**d**) of *m*-BADCy resin at different testing frequency

the formation of the symmetric triazine structure [32]. Besides, the fluorine-containing P(PFS-*co*-GMA) has a large free volume, which causes the decrease of the polarization, thus resulting the lower ε and tanδ. However, when the mass fraction of P(PFS-*co*-GMA) is further increased to 20 wt%, the excess epoxy groups in P(PFS-*co*-GMA) react with –OCN groups of BADCy forming a considerable amount of larger polarized oxazolidinone structure, which destructs the highly symmetrical triazine ring of BADCy resin, thus increasing ε and tanδ of the *m*-BADCy resin. In addition, the ε of pure BADCy resin and *m*-BADCy resin decreases with the increase of testing frequency. The main reason is that, at lower external electric field frequency, a variety of polarization (orientation, atomic, and electronic polarization) could keep up to the electric field change. However, orientation polarization requires longer relaxation time which gradually lags behind the external electric field change when increasing the electric field frequency, resulting in the decreased ε.

Figure 3 c and d show the amount of P(PFS-*co*-GMA) affecting on wave transmittance ($|T|^2$), wave reflectivity ($|\Gamma|^2$), and energy loss (A) of *m*-BADCy resin at different frequencies. The calculation equation for $|T|^2$, $|\Gamma|^2$, and A is shown in Eq. S1 – S4 [43]. With increasing the content of P(PFS-*co*-GMA), the $|T|^2$ of *m*-BADCy resin increases firstly and then decreases, while the $|\Gamma|^2$ displays a contrast trend. When the amount of P(PFS-*co*-GMA) reaches 15 wt%, the $|T|^2$ of *m*-BADCy resin increases to the maximum value of 94.5% at 1 MHz, higher than that of pure BADCy resin (92.9%). Simultaneously, the corresponding $|\Gamma|^2$ is reduced to 5.5%, lower than that of pure BADCy resin (7.1%). It may be explained by impedance matching theory, where the smaller the impedance difference of the load phase and the transmission phase is, the less reflection

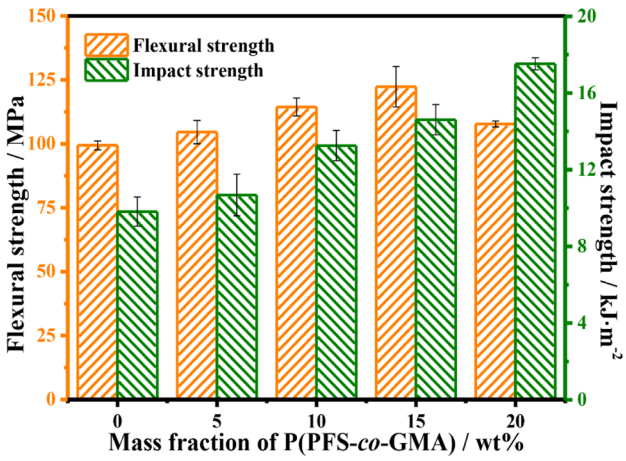

Fig. 4 Influence of P(PFS-*co*-GMA) mass fraction on the mechanical properties of *m*-BADCy resin

of the electromagnetic waves occurs [44–47]. Therefore, the impedance difference of *m*-BADCy resin and transmission phase (air) becomes smaller as ε of *m*-BADCy resin decreases, thus resulting in lower $|\Gamma|^2$ and higher $|T|^2$. Additionally, the *A* of pure BADCy and *m*-BADCy resin is much lower than $|\Gamma|^2$ (less than 0.7×10^{-3}%), suggesting the reflection loss is the main way causing the energy reduction of the electromagnetic waves.

3.3 Mechanical properties of *m*-BADCy resin

Figure 4 shows the amount of P(PFS-*co*-GMA) influencing on the mechanical properties of *m*-BADCy resin. As mass fraction for P(PFS-*co*-GMA) increases, the flexural strength of *m*-BADCy resin increases first and then decreases. Whereas, the impact strength of *m*-BADCy resin keeps increasing as the content of P(PFS-*co*-GMA) increases. When the content of P(PFS-*co*-GMA) is 15 wt%, *m*-BADCy resin reaches the optimal flexural strength of 122.4 MPa, increased by 23.1% compared with 99.4 MPa of pure BADCy resin. The corresponding impact strength of *m*-BADCy resin reaches 14.6 kJ/m^2, increased by 49.0% compared with pure BADCy (9.8 kJ/m^2). Pure BADCy displays a smooth and brittle fracture surface (Fig. 5a) indicating that there is almost no plastic deformation in the process of fracture propagation. With the addition of P(PFS-*co*-GMA), the fracture surface of *m*-BADCy resin appears irregularly corrugated and the roughness gradually

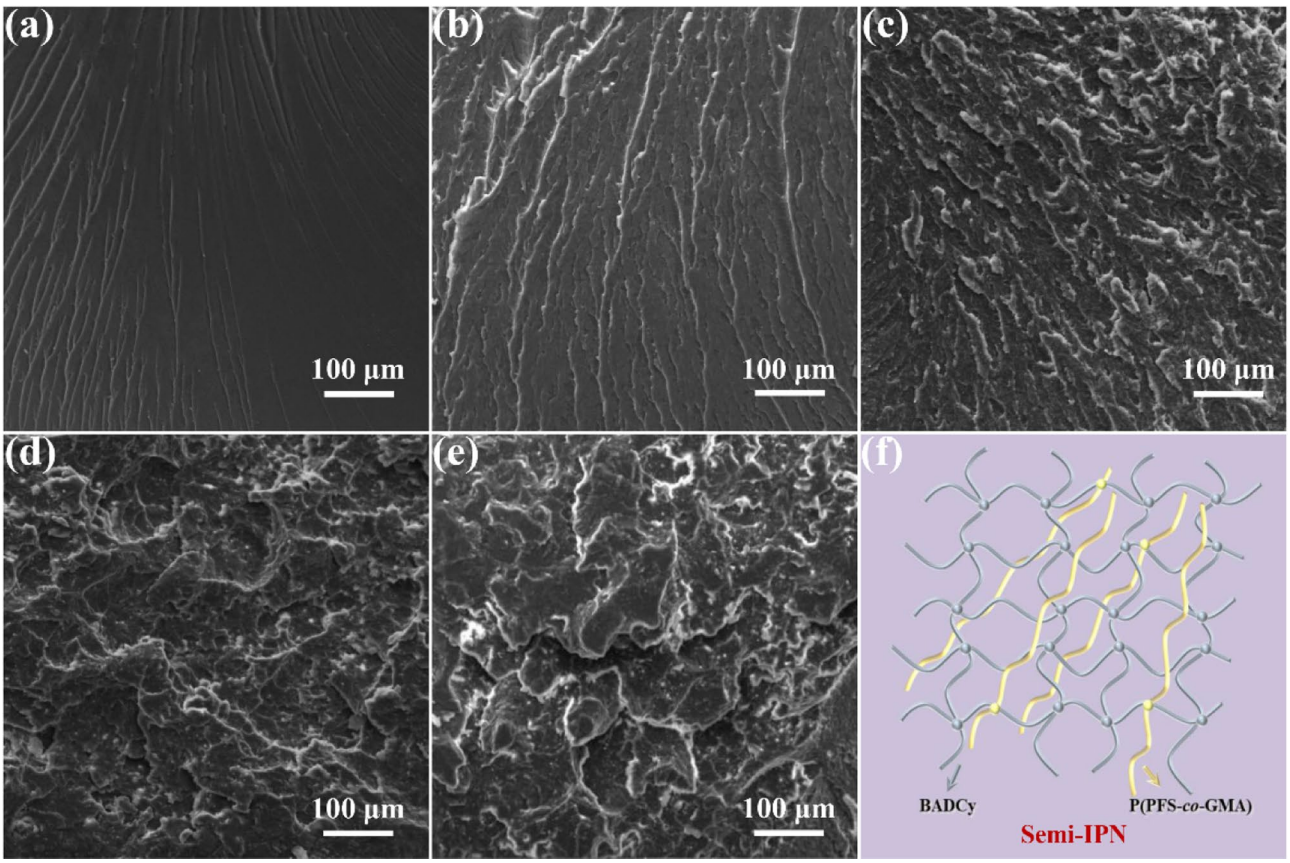

Fig. 5 SEM morphologies of impact fractures for *m*-BADCy resin with different mass fraction of P(PFS-*co*-GMA): 0 (**a**), 5 (**b**), 10 (**c**), 15 (**d**), and 20 wt% (**e**); schematic diagram showing the formation of semi-IPN structure in *m*-BADCy resin (**f**)

increases (Fig. 5b–e), which is in favor of enhancing the mechanical properties. Furthermore, the phenomenon of stress whitening becomes more obvious, also indicating the transition from brittle fracture to ductile fracture. The increased mechanical properties can be mainly ascribed to the formed semi-IPN structure between the cured BADCy resin and the P(PFS-*co*-GMA) as shown in Fig. 5f. Besides, the reaction of epoxy groups in P(PFS-*co*-GMA) with –OCN groups in *m*-BADCy resin increases the compatibility of the flexible five-membered ring oxazolidinone. Furthermore, fluorine atoms have big free volume which increases flexibility of chain segment in the *m*-BADCy resin system. These factors are beneficial to improving the impact strength of *m*-BADCy resin. However, when the addition of P(PFS-*co*-GMA) increases to 20 wt%, the excessive oxazolidinone has an adverse effect on the flexural strength of *m*-BADCy resin.

Table 1 Thermal data of pure BADCy and *m*-BADCy resin. $T_{HRI}=0.49\times[T_5+0.6\times(T_{30}-T_5)]$. T_5 and T_{30} represent thermal decomposition temperature corresponding to the sample weight loss of 5% and 30%, respectively.

Samples	Weight loss temperature/°C		T_{HRI}*/°C	T_g/°C
	T_5	T_{30}		
Pure BADCy	362.8	458.2	205.8	260.4
5 wt% P(PFS-*co*-GMA)/BADCy	373.4	463.6	209.5	265.6
10 wt% P(PFS-*co*-GMA)/BADCy	363.4	465.2	208.0	252.7
15 wt% P(PFS-*co*-GMA)/BADCy	356.8	454.9	203.7	248.5
20 wt% P(PFS-*co*-GMA)/BADCy	350.8	444.2	199.4	248.1

3.4 Thermal properties of *m*-BADCy resin

Dynamic mechanical analysis (DMA) and thermal gravimetric analyses (TGA) of *m*-BADCy resin are shown in Fig. 6a–b, and the respective thermal data are shown in Table 1. Glass transition temperature (T_g) of *m*-BADCy resin displays an increasing trend followed by decreasing as P(PFS-*co*-GMA) increases from 0 to 5 wt% and from 5 to 20 wt%, respectively. When the mass fraction of P(PFS-*co*-GMA) is 5 wt%, the T_g of *m*-BADCy resin rises to the maximum value of 265.6 °C, higher than that of pure BADCy resin (260.4 °C). The reason is that the introduction of a lower content epoxy groups promotes the curing of *m*-BADCy resin and increases the crosslinking density, thereby increasing the T_g of *m*-BADCy resin. However, the T_g of *m*-BADCy resin is decreased to 248.5 °C when the mass fraction of P(PFS-*co*-GMA) goes up to 15 wt%. This is mainly caused by the reaction of excess epoxy groups of GMA with the –OCN groups of BADCy which forms flexible five-membered ring oxazolidinone. It will cause the destruction of rigidly regular triazine ring structure, thereby reducing the T_g.

From Fig. 6b and Table 1, the T_5, T_{30}, and $T_{\text{Heat-resistance index}}$ (T_{HRI}) [48] values of *m*-BADCy resin increase first before decrease with increasing the mass fraction of P(PFS-*co*-GMA). The T_{HRI} value of *m*-BADCy resin with 15 wt% P(PFS-*co*-GMA) is 203.7 °C, slightly lower than that of pure BADCy (205.8 °C). On the one hand, the excellent thermal oxidation resistance improves the heat resistance of *m*-BADCy resin owing to the high carbon–fluorine bond energy. On the other hand, the formed excess five-membered ring oxazolidinone with the increase of P(PFS-*co*-GMA) has relatively poor heat resistance. This factor plus the decreased

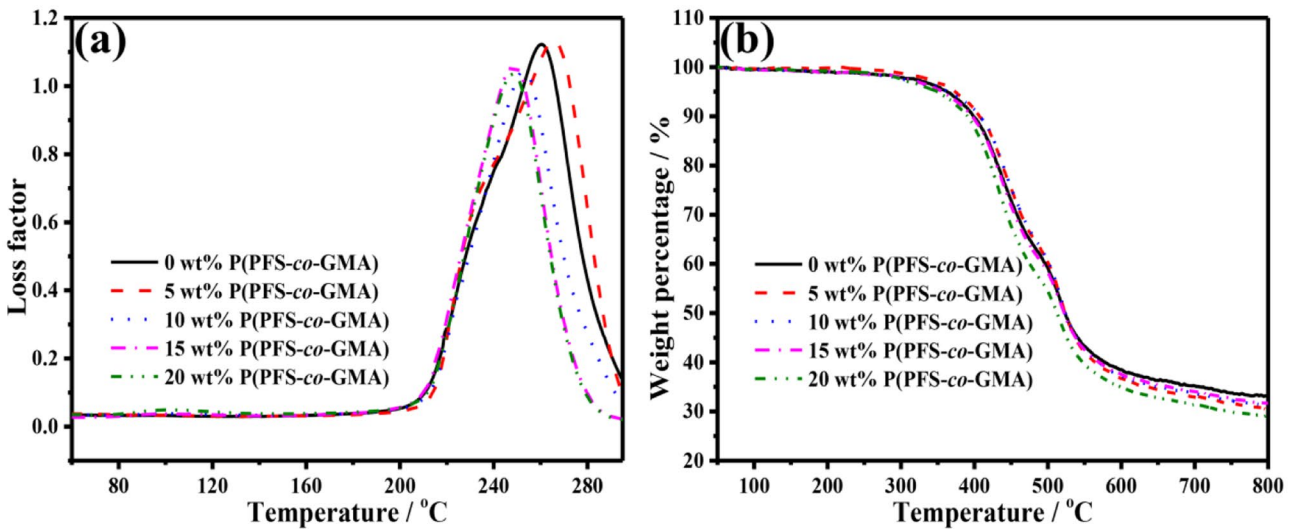

Fig. 6 DMA **(a)** and TGA **(b)** curves of pure BADCy and *m*-BADCy resin

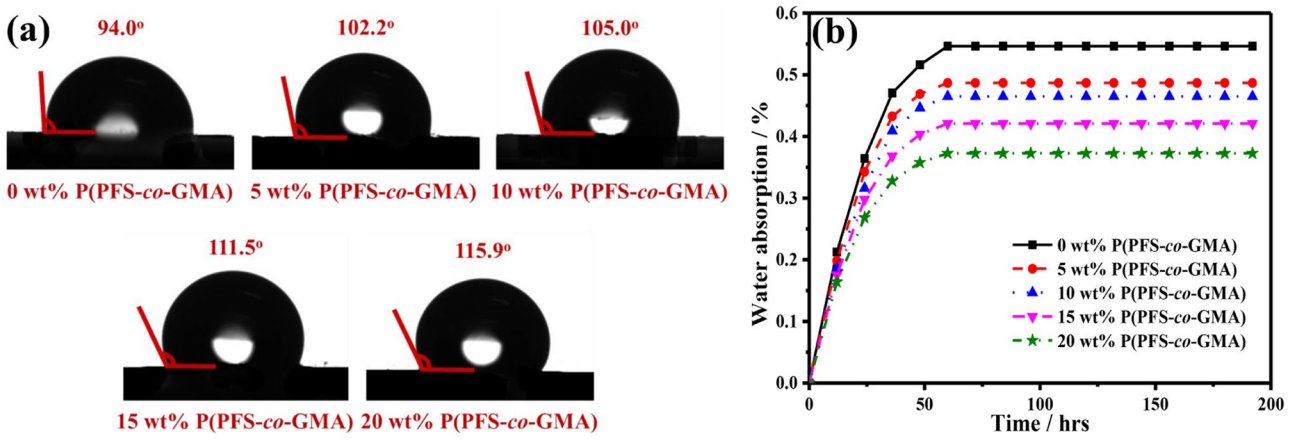

Fig. 7 Water contact angles (**a**) and water absorption (**b**) of pure BADCy and *m*-BADCy resin

crosslinking density of *m*-BADCy resin offset the improving effect and thus deteriorate the heat resistance of the resin.

*$T_{HRI} = 0.49 \times [T_5 + 0.6 \times (T_{30} - T_5)]$. T_5 and T_{30} represent thermal decomposition temperature corresponding to the sample weight loss of 5% and 30%, respectively.

3.5 Water resistance of *m*-BADCy resin

Figure 7a and b respectively demonstrate the amount of P(PFS-*co*-GMA) influencing on the contact angle and water absorption of *m*-BADCy resin. The contact angle of *m*-BADCy resin increases with increasing the addition of P(PFS-*co*-GMA) (Fig. 7a). And the contact angle of *m*-BADCy resin is increased to 111.5° with 15 wt% P(PFS-*co*-GMA), larger than that of pure BADCy resin (94.0°). Improved hydrophobicity of *m*-BADCy resin corresponds to the strong binding force of the carbon–fluorine bond and the very low surface energy. In addition, as demonstrated from Fig. 7b, the water absorption of pure BADCy and *m*-BADCy resin increases with prolonging the immersing time in water and reaches saturation after 48 h. Notably, *m*-BADCy resin displays a slower water absorption rate and lower final saturation absorption compared to pure BADCy resin. When the content of P(PFS-*co*-GMA) reaches 15 wt%, the saturated water absorption of *m*-BADCy resin drops to 0.42%, lower than that of pure BADCy resin (0.55%). It can also be ascribed to the low free energy of carbon–fluorine bond, which makes *m*-BADCy resin highly hydrophobic.

4 Conclusion

In summary, a novel linear random copolymer of P(PFS-*co*-GMA) was successfully designed and synthesized via RAFT polymerization. The obtained *m*-BADCy resin with 15 wt% P(PFS-*co*-GMA) demonstrated the optimal comprehensive properties. ε and tanδ were 2.59 and 0.0053, respectively, lower than that of pure BADCy resin (2.97 and 0.0090). The corresponding wave transmittance ($|T|^2$) increased from 92.9% of pure BADCy resin to 94.5%. Meanwhile, the flexural and impact strength increased to 122.4 MPa and 14.6 kJ/m^2, increased by 23.1% and 49.0% compared with pure BADCy resin (99.4 MPa and 9.8 kJ/m^2), respectively. Simultaneously, *m*-BADCy resin demonstrated excellent thermal stability (T_{HRI} of 203.7 °C) and water resistance (contact angle of 111.5° and the saturated water absorption rate of 0.42%) at this point.

Supplementary Information The online version contains supplementary material available at https://doi.org/10.1007/s42114-021-00349-3.

Funding This research was financially supported by the National Scientific Research Project (Basis Strengthening Plan) and China Postdoctoral Science Foundation (2019M653735). C. Q. and L. L. acknowledge the Undergraduate Innovation & Business Program in Northwestern Polytechnical University for funding (S202110699153 and S202110699571). This work is also financially supported by Polymer Electromagnetic Functional Materials Innovation Team of Shaanxi Sanqin Scholars.

Declarations

Conflict of interest The authors declare no competing interests.

References

1. Chen Z, Luo J, Huang Z, Cai C, Tusiime R, Li Z, Wang H, Cheng C, Liu Y, Sun Z, Zhang H, Yu J (2020) Synergistic toughen epoxy resin by incorporation of polyetherimide and amino groups grafted MWCNTs. Compos Commun 21:100377.
2. Zhou Y, Liu F, Chen C-Y (2019) Use of BN-coated copper nanowires in nanocomposites with enhanced thermal conductivity and electrical insulation. Adv Compos Hybrid Mater 2(1):46–50
3. Han X, Yuan L, Gu A, Liang G (2018) Development and mechanism of ultralow dielectric loss and toughened bismaleimide resins with high heat and moisture resistance based on unique

amino-functionalized metal-organic frameworks. Compos Part B-Eng 132:28–34
4. Pisani W A, Radue M S, Patil S U, Odegard G M (2021) Interfacial modeling of flattened CNT composites with cyanate ester and PEEK polymers. Compos Part B-Eng 211:108672.
5. Tang L, Zhang J, Gu J (2021) Random copolymer membrane coated PBO fibers with significantly improved interfacial adhesion for PBO fibers/cyanate ester composites. Chinese J Aeronaut 34(2):659–668
6. Wang B, Zhang Z, Pei Z, Qiu J, Wang S (2020) Current progress on the 3D printing of thermosets. Adv Compos Hybrid Mater 3(4):462–472
7. Li W, Huang W, Kang Y, Gong Y, Ying Y, Yu J, Zheng J, Qiao L, Che S (2019) Fabrication and investigations of G-POSS/cyanate ester resin composites reinforced by silane-treated silica fibers. Compos Sci Technol 173:7–14
8. Zhang X, Wang F, Zhu Y, Qi H (2019) Cyanate ester composites containing surface functionalized BN particles with grafted hyperpolyarylamide exhibiting desirable thermal conductivities and a low dielectric constant. RSC Adv 9(62):36424–36433
9. Gu J, Xu S, Zhuang Q, Tang Y, Kong J (2017) Hyperbranched polyborosilazane and boron nitride modified cyanate ester composite with low dielectric loss and desirable thermal conductivity. IEEE T Dielect El In 24(2):784–790
10. Arumugam V, Kanthapazham R, Zherebtsov DA, Kalimuthu K, Pichaimani P, Muthukaruppan A (2021) Fluorine free TiO_2/cyanate ester coated cotton fabric with low surface free energy and rough surface for durable oil-water separation. Cellulose 28(8):4847–4863
11. Chandrasekaran S, Duoss EB, Worsley MA, Lewicki JP (2018) 3D printing of high performance cyanate ester thermoset polymers. J Mater Chem A 6(3):853–858
12. Tang L, Dang J, He M, Li J, Kong J, Tang Y, Gu J (2019) Preparation and properties of cyanate-based wave-transparent laminated composites reinforced by dopamine/POSS functionalized Kevlar cloth. Compos Sci Technol 169:120–126
13. Li S, Zhu Y, Wang Y, Wang B, Huang Y, Yu T (2021) Cyanate ester resin based composites with high toughness and low outgassing performances. Compos Commun 23:100574.
14. Vashchuk A, de Anda AR, Starostenko O, Grigoryeva O, Sotta P, Rogalsky S, Smertenko P, Fainleib A, Grande D (2018) Structure-property relationships in nanocomposites based on cyanate ester resins and 1-heptyl pyridinium tetrafluoroborate ionic liquid. Polymer 148:14–26
15. Fang L, Zhou J, Tao Y, Wang Y, Chen X, Chen X, Hou J, Sun J, Fang Q (2019) Low dielectric fluorinated polynorbornene with good thermostability and transparency derived from a biobased allylphenol (eugenol). ACS Sustain Chem Eng 7(4):4078–4086
16. He F, Gao Y, Jin K, Wang J, Sun J, Fang Q (2016) Conversion of a biorenewable plant oil (anethole) to a new fluoropolymer with both low dielectric constant and low water uptake. ACS Sustain Chem Eng 4(8):4451–4456
17. Jiang Q, Zhang W, Hao J, Wei Y, Mu J, Jiang Z (2015) A unique "cage-cage'' shaped hydrophobic fluoropolymer film derived from a novel double-decker structural POSS with a low dielectric constant. J Mater Chem C 3(44):11729–11734
18. Hu J, Gu A, Jiang Z, Liang G, Zhuo D, Yuan L, Zhang B, Chen X (2012) High efficiency synthesis of octavinylsilsesquioxanes and its high performance hybrids based on bismaleimide-triazine resin. Polym Advan Technol 23(8):1219–1228
19. Zhang Z, Pei J, Liang G, Yuan L (2011) Methyl silsesquioxane/cyanate ester resin organic-inorganic hybrids with low dielectric constant. J Appl Polym Sci 121(2):1004–1012
20. Devaraju S, Vengatesan MR, Selvi M, Song JK, Alagar M (2013) Mesoporous silica reinforced cyanate ester nanocomposites for low *k* dielectric applications. Micropor Mesopor Mat 179:157–164
21. Wu Z, Zhao L, Qi L, Jiao J (2017) Improved cyanate resin with low dielectric constant and high toughness prepared using inorganic-organic hybrid porous silica. Chem Lett 46(1):139–142
22. Guo X, Deng H, Fu Q (2020) An unusual decrease in dielectric constant due to the addition of nickel hydroxide into silicone rubber. Compos Part B-Eng 193:108006.
23. Liu J, Fu Y, Fu X, Li Y, Liang D, Song Y, Pan C, Yu G, Xiao X (2016) Nanoscale porous triazine-based frameworks with cyanate ester linkages for efficient drug delivery. RSC Adv 6(25):20834–20842
24. Milliman HW, Boris D, Schiraldi DA (2012) Experimental determination of hansen solubility parameters for select POSS and polymer compounds as a guide to POSS-polymer interaction potentials. Macromolecules 45(4):1931–1936
25. Liu Z, Yuan L, Liang G, Gu A (2015) Tough epoxy/cyanate ester resins with improved thermal stability, lower dielectric constant and loss based on unique hyperbranched polysiloxane liquid crystalline. Polym Advan Technol 26(12):1608–1618
26. Ye J, Liang G, Gu A, Zhang Z, Han J, Yuan L (2013) Novel phosphorus-containing hyperbranched polysiloxane and its high performance flame retardant cyanate ester resins. Polym Degrad Stabil 98(2):597–608
27. Wang B, Shang Y-R, Ma Z, Pan L, Li Y-S (2017) Non-porous ultra low dielectric constant materials based on novel silicon-containing cycloolefin copolymers with tunable performance. Polymer 116:105–112
28. Ariraman M, Sasikumar R, Alagar M (2015) Hybridization of PDMS based cyanate ester and DGEBA for radiation resistant and microelectronics applications. RSC Adv 5(78):63641–63649
29. Liu J, Meng Q, Li L, Lu G, Yuan H, Cui L, Liu X, Mu H, Ji J, Zhou D, Wang Z, Yan J (2020) A high-performance polycyanurate network derived from 4, 4'-biscyanato-2, 2'-trifluoromethylbiphenyl. Polym Chem 11(4):784–788
30. Tao Y, Zhou J, Fang L, Wang Y, Chen X, Chen X, Hou J, Sun J, Fang Q (2019) Fluoro-containing polysiloxane thermoset with good thermostability and acid resistance based on the renewable multifunctional vanillin. ACS Sustain Chem Eng 7(7):7304–7311
31. Yuan C, Jin K, Li K, Diao S, Tong J, Fang Q (2013) Non-porous low-*k* dielectric films based on a new structural amorphous fluoropolymer. Adv Mater 25(35):4875–4878
32. Wang C, Tang Y, Zhou Y, Zhang Y, Kong J, Gu J, Zhang J (2021) Cyanate ester resins toughened with epoxy-terminated and fluorine-containing polyaryletherketone. Polym Chem 12(26):3753–3761
33. Liu Z, Fan X, Zhang J, Yang Z, Tang Y, Li J, Kong J, Gu J (2021) Improving the comprehensive properties of PBO fibres/cyanate ester composites using a hyperbranched fluorine and epoxy containing PBO precursor. Compos Part A-Appl S 150:106596.
34. Tang L, Zhang J, Tang Y, Kong J, Liu T, Gu J (2021) Polymer matrix wave-transparent composites: A review. J Mater Sci Technol 75:225–251
35. Yin Q, Alcouffe P, Beyou E, Charlot A, Portinha D (2018) Controlled perfluorination of poly(2, 3, 4, 5, 6-pentafluorostyrene) (PPFS) and PPFS-functionalized fumed silica by thiol-para-fluoro coupling: Towards the design of self-cleaning (nano) composite films. Eur Polym J 102:120–129
36. Atanasov V, Kerres J (2011) Highly phosphonated polypentafluorostyrene. Macromolecules 44(16):6416–6423
37. Atanasov V, Oleynikov A, Xia J, Lyonnard S, Kerres J (2017) Phosphonic acid functionalized poly(pentafluorostyrene) as polyelectrolyte membrane for fuel cell application. J Power Sources 343:364–372
38. Bucholz TL, Li SP, Loo Y-L (2008) Ultra-low-*k* materials derived from poly(D, L-lactide-*b*-pentafluorostyrene) diblock copolymers. J Mater Chem 18(5):530–536

39. Fu GD, Kang ET, Neoh KG, Lin CC, Liaw DJ (2005) Rigid fluorinated polyimides with well-defined polystyrene/poly(pentafluoro styrene) side chains from atom transfer radical polymerization. Macromolecules 38(18):7593–7600
40. Inamdar A, Cherukattu J, Anand A, Kandasubramanian B (2018) Thermoplastic-toughened high-temperature cyanate esters and their application in advanced composites. Ind Eng Chem Res 57(13):4479–4504
41. Liu J, Fan W, Lu G, Zhou D, Wang Z, Yan J (2019) Semi-interpenetrating polymer networks based on cyanate ester and highly soluble thermoplastic polyimide. Polymers 11(5):862
42. Zhou Z-X, Li Y, Zhong J, Luo Z, Gong C-R, Zheng Y-Q, Peng S, Yu L-M, Wu L, Xu Y (2020) High-performance cyanate ester resins with interpenetration networks for 3D printing. ACS Appl Mater Inter 12(34):38682–38689
43. Liu Z, Zhang J, Tang Y, Xu J, Ma H, Kong J, Gu J (2021) Optimization of PBO fibers/cyanate ester wave-transparent laminated composites via incorporation of a fluoride-containing linear interfacial compatibilizer. Compos Sci Technol 210:108838.
44. Zhao B, Bai Z, Guo X, Zhang R, Jiang Q, Guo Z (2021) Poly(vinylidene fluoride)/Cu@Ni anchored reduced-graphene oxide composite films with folding movement to boost microwave absorption properties. Engineered Science, https://doi.org/10.30919/esee8c488.
45. Osipov AV (2014) Minimum reflection properties of planar impedance-matched boundaries. Ieee T Antenn Propag 62(11):5666–5670
46. Wu N, Zhao B, Liu J, Li Y, Chen Y, Chen L, Wang M, Guo Z (2021) MOF-derived porous hollow Ni/C composites with optimized impedance matching as lightweight microwave absorption materials. Adv Compos Hybrid Mater 4:707–715
47. Xie P, Liu Y, Feng M, Niu M, Liu C, Wu N, Sui K, Patil RR, Pan D, Guo Z, Fan R (2021) Hierarchically porous Co/C nanocomposites for ultralight high-performance microwave absorption. Adv Compos Hybrid Mater 4(1):173–185
48. Zhao J, Zhang J, Wang L, Li J, Feng T, Fan J, Chen L, Gu J (2020) Superior wave-absorbing performances of silicone rubber composites via introducing covalently bonded SnO_2@MWCNT absorbent with encapsulation structure. Compos Commun 22:100486.